JOURNAL OF REINFORCED PLASTICS & COMPOSITES

Original article

Analysis and structural evaluation of seawater-aged composite tidal turbine blades using multi-walled carbon nanotubes and acoustic emission

Journal of Reinforced Plastics and Composites
2026, Vol. 45(1-2) 308–320

DOI: 10.1177/07316844241274608
journals.sagepub.com/home/jrp
Sage

Eduardo José-Trujillo[1], Carlos Rubio-González[2] and Julio A. Rodríguez-González[3]

Abstract

The main objective of this research was to evaluate the piezoresistive response and mechanical performance of seawater-aged blades manufactured with glass fiber/epoxy resin incorporating multi-walled carbon nanotubes (MWCNTs). MWCNTs content was 0.75 wt. %, which was sufficient to form an electric percolation network. MWCNTs were dispersed in the fiber using the spray-coating method, allowing the entire blade outer surface to gain strain self-sensing capability. Exposure of the blades with and without MWCNT to seawater caused a moisture absorption of 1.67% and 1.56%, respectively. This caused damage such as matrix cracking, and fiber/matrix interfacial debonding. These effects were manifested by an increase in tip displacement of 13% and 1.43% in the blades with and without MWCNTs, also local deformations on the blade increased. The MWCNTs induced a positive effect on piezoresistive capability, resulting in the development of sensitivity to deformation. This showed that MWCNTs in the specified content is efficient for damage detection in complex structural components even after seawater aging while retaining maximum electrical resistance change of 0.45% and 0.26% on the tensile and compressive side, respectively. With acoustic emission (AE), it was confirmed that the presence of MWCNTs acts as toughening mechanisms reducing damage such as micro-cracks in the matrix.

Keywords

Acoustic emission, composite laminate, hydrokinetic turbine blade, multi-walled carbon nanotubes, piezoresistive response, seawater aging

Introduction

With the growing global trend for reducing the use of fossil fuels, which are the main generators of carbon dioxide emissions that cause adverse effects on the environment, such as the greenhouse effect, and which has been increasing in recent years,[1–3] one of the alternatives to mitigate them is to make use of clean energy or alternative energies.[4–6] One of the ways to generate clean energy is through the use of sea water resources, such as waves, ocean currents, saline gradients, and temperature gradients.[7–9] This energy harnessing, specifically the kinetic energy from ocean currents, can be converted into electrical energy through the implementation of horizontal axis hydrokinetic turbines (HATT) or vertical axis hydrokinetic turbines (VATT). Although this technology may be 20 years behind the development of wind energy, it has been demonstrated to progress beyond the conceptual stage.[10]

The main component of hydrokinetic turbines is the blade, which, being a critical structural element,[11,12] its durability is essential for the turbine's operation and must have a certain resistance to the corrosive marine environment,[13,14] and considering that the duration of a hydrokinetic turbine is around 20 years,[15,16] these elements must preserve their properties throughout that time. In addition to the adverse environment in which the blades operate, they are also exposed to potential damage from low-speed impacts caused by floating or submerged debris, underwater

[1]Departamento de Ingeniería Mecánica, Centro de Ingeniería y Desarrollo Industrial, Querétaro, Mexico
[2]Escuela de Ingeniería y Ciencias, Tecnológico de Monterrey, Querétaro, Mexico
[3]Departamento de Tecnologías Estratégicas y Posgrado, Centro de Ingeniería y Desarrollo Industrial, Querétaro, Mexico

Corresponding author:
Eduardo José-Trujillo, Departamento de Ingeniería Mecánica, Centro de Ingeniería y Desarrollo Industrial, Av. Pie de la Cuesta #702, Col. Desarrollo San Pablo, Querétaro 76125, México.
Email: eduardo.jose@cidesi.edu.mx

cables, ice, marine animals, collisions with vessels, and docks.[17] The blades are also exposed to high levels of loads due to current velocities and water density; they also experience cavitation and wear caused by turbulence generated by the currents.[18] Being immersed for extended periods in humid environments, the blades undergo a phenomenon known as aging. As a result, unscheduled maintenance requirements for HATTs are largely due to a large blade failure rate.[19] Because of this, it is important to mention that currently the material most commonly used for manufacturing blades is glass fiber-reinforced polymers (GFRP),[20] due to their elevated mechanical properties such as strength, rigidity, low density, fatigue resistance, and corrosion resistance.[21] This combination of characteristics, among other advantages, has made GFRP one of the best choices for composite materials in the design of marine structural components, not only for hydrokinetic turbine blades but also for boats, ships, platforms, and various other applications.[22]

The aging of marine components with polymeric matrices is a serious problem that leads to the degradation of mechanical properties,[23,24] thereby reducing the expected element's lifespan and amplifying failure modes that occur prematurely and can be catastrophic for the structural integrity of marine elements.[18] Added to these structural and physical problems, there is also a cost associated with the deployment, maintenance and recovery of HATTs that are installed in hostile underwater environments that make reliability and preservation the main concerns of designers and researchers.[25]

Because the interest of researchers in the study of marine effects on structural components has been increasing, some authors, such as Shi et al.,[26] have focused their research on studying phenomena that occur during the operation of the blades, such as cavitation. Additionally, Ghoil and Saini focused their research on erosion, which is caused by the dynamic action of sand flowing with the water current, causing wear, this wear reduces the efficiency and lifespan of the turbine, leading to operational issues, premature maintenance, and, in turn, economic losses.[27] In this regard, Hassan also studied the erosion mechanisms in composite materials and the influence of immersion in seawater on the mechanical properties of hydrokinetic turbine blades.[28]

But some other authors have conducted a more comprehensive investigation by experimentally[29] and numerically studying the structural behavior of the blades through finite element analysis (FEA). This is the case of Jaksic et al.,[30] who based their experiment on large-scale blades, where they studied the materials, performed numerical analysis, conducted static and fatigue experiments on the blades. On the other hand, Gonabadi et al.[31] established a design methodology based on hydrodynamic models by applying the finite element analysis (FEA) method to experimentally validate blades manufactured with composite materials, the aim was to predict the structural performance of the blades under extreme loading conditions. Fagan et al.[32] developed a design methodology based on damage mechanics to assess blades of hydrokinetic turbines. On the other hand, Kennedy et al.[33] presented a study on the fatigue of glass fiber-reinforced polymers (GFRP) subjected to accelerated aging. They established that moisture saturation has a detrimental effect on the fatigue strength of the composite for its use in marine energy structures. Nachtane et al.[34] used the most advanced finite element features available to investigate the effects of environmental exposure on the mechanical properties of a composite hydrokinetic turbine.[34]

Regarding their contribution, Davies et al.[35] investigated the behavior of blades exposed to the marine environment, for this purpose they proposed several material alternatives to be investigated through tests on full-scale blades.[35] Also Robin et al. have conducted studies on structural components to evaluate their in-plane and out-of-plane performance when the elements have been aged with seawater.[36] In this sense, other researchers have also studied alternatives to reduce the negative impact of the marine environment on structures by incorporating cores.[37] Jiang et al. have contributed with extensive research on the effect of seawater on the mechanical resistance of a blade; they concluded that seawater negatively impacts the resistance of the blade, in terms of the stiffness and risk of failure of the composites. However, the results showed that the blade can withstand the design loads and that its operation is guaranteed during its useful life despite the absorption of seawater.[38] Despite the studies found in the literature on the topic of hydrothermal aging in composite structures, it is still considered a challenging topic because it has not been fully understood and should not be underestimated and requires special attention and further studies.[39]

As observed, there is a growing trend towards harnessing marine currents through energy converters. This has raised significant technological concerns, such as structural health monitoring (SHM) for detecting failures in the blades. These failures can cause disruptions in the efficiency of turbines when they are in operation. As a result, various failure detection methods have been under development, and one of them involves detecting failures through sensors incorporated into structural elements, such as the voltages and phase currents of the generator windings.[40] Another type of sensor that has also been explored and is inherently integrated into the manufacturing of structures is fiber-based sensors, forming the Bragg grating grid.[41,42] In general, structural health monitoring involves a variety of sensors (strain, vibration, temperature, GPS) that can be permanently installed on the elements or embedded within their structure.[43–47] However, integrating any type of sensor

into the structure of an element can affect its mechanical properties, particularly those of the blades, and as a result, their mechanical performance may be severely compromised.[48] Another technique to monitor SHM of components in operation is acoustic emission (AE). It is based on the transient waves produced by the appearance of internal defects; features of AE signals may provide information about the damage mechanisms and defect evolution.[49] Lately this approach has been applied in systems and structures for the generation, transmission, transformation, and storage of renewable energy, being able to monitor the structural condition and diagnose failures in the systems and structures.[50]

In recent times, the use of nanomaterials, specifically multi-wall carbon nanotubes (MWCNTs), has been promoted with a dual purpose. On the one hand, to enhance or maintain mechanical properties intact and on the other hand, to reinforce electrical properties as a means for structural health monitoring of components.[48] The efficient incorporation of MWCNTs into the fiber of GFRP leads to the formation of electrical percolation networks, providing the ability to be used as piezoresistive sensors without affecting the mechanical properties.[51–53] MWCNTs can be incorporated into the composite using two approaches, the first by mixing the nanomaterials in the resin[54,55] and the second by dispersing the nanomaterials directly in the reinforcement.[56–58] The greatest challenges when using the second type of dispersion consist primarily of achieving uniform coating on the fiber, obtaining good interlaminar adhesion and making the process scalable at a minimum cost.[54] In this case, new avenues for the development of minimally invasive and high-performance sensors for process monitoring have been opened, since the integrated nanomaterials impart structure-dependent electrical characteristics.[48] Such is the case of Rubio-González et al. who developed a composite material blade with the incorporation of MWCNTs, with the aim of obtaining a blade capable of being self-sensitive to deformation due to external loads.[59]

Although piezoresistive capabilities for structural health monitoring in seawater-aged specimens have been studied,[60] there is still some uncertainty about how these piezoresistive properties will behave after aging. It remains to be confirmed whether these properties remain active after seawater aging in more complex structural elements, such as a hydrokinetic turbine blade. Given this context, this paper firstly presents a study on the aging of a hydrokinetic turbine blade with the incorporation of MWCNTs in its matrix. Subsequently, static tests were conducted using relevant standards to investigate the piezoresistive response of the aged blade. The results of the mechanical and piezoresistive response were complemented with acoustic emission studies, visual inspection and fractography by scanning electron microscope for the damage analysis.

Experimental

Materials

For the manufacturing of the blades, Epolam 2040 epoxy resin was used, which was mixed with the Epolam 2040 hardener at a ratio of 100:30 by weight, these materials were supplied by Axson Technologies (USA). Unidirectional (UD) and TRIAX fiber fabrics with a density of 2.62 g/cm^3 from Axson Technologies (USA) were also employed. For the blade core, R-3318 polyurethane foam was used, with a density of 288 kg/m^3. The foam core of polyurethane (PU) was purchased from General Plastic Manufacturing Company (USA). Multi-walled carbon nanotubes (MWCNTs) with an average length of 1–10 μm and an outer diameter of 10–35 nm were used, with a purity of >90%. The MWCNTs were produced by chemical vapor deposition and purchased from Sunnano (China).

Fabrication of multifunctional tidal turbine blade

A novel method was employed to manufacture the blades used in the experiments,[59] which involves a one-step injection process using the Vacuum Assisted Resin Transfer Moulding (VARTM) method. In this process, a split metal mold with the blade's geometry inside and a polyurethane foam core specially machined to the shape of the blade was used. During manufacturing, the outer layer of the blade's fiberglass fabric was impregnated with MWCNTs, following the process reported by Rubio et al. This process involves the dispersion of the MWCNTs/ethanol mixture using a professional airbrush, with an MWCNT content of 0.75 wt. %. After curing, excess resin at the edges of the blades was trimmed. Four blades were prepared and they are shown in Figure 1(a); Blade 1 and Blade 2 were manufactured without MWCNTs, while Blade 3 and Blade 4 contain MWCNTs. Additionally, Blade 2 and Blade 4 underwent a seawater aging process. A summary of the manufacturing conditions is shown in Table 1.

Seawater aging

The seawater aging process was conducted by keeping the blades submerged in a thermostatic bath with artificial seawater at a temperature of 60°C for 365 days. Before immersion, the blades were weighed using a Mettler Toledo scale with a 5 kg capacity and an accuracy of 0.01 g, the same scale was used to measure the increase in the amount of moisture absorbed by the blade at certain time intervals. The percentage of moisture absorption (M_t) is determined by the following equation.[61]

$$M_t = \frac{W_t - W_0}{W_0} \times 100 \quad (1)$$

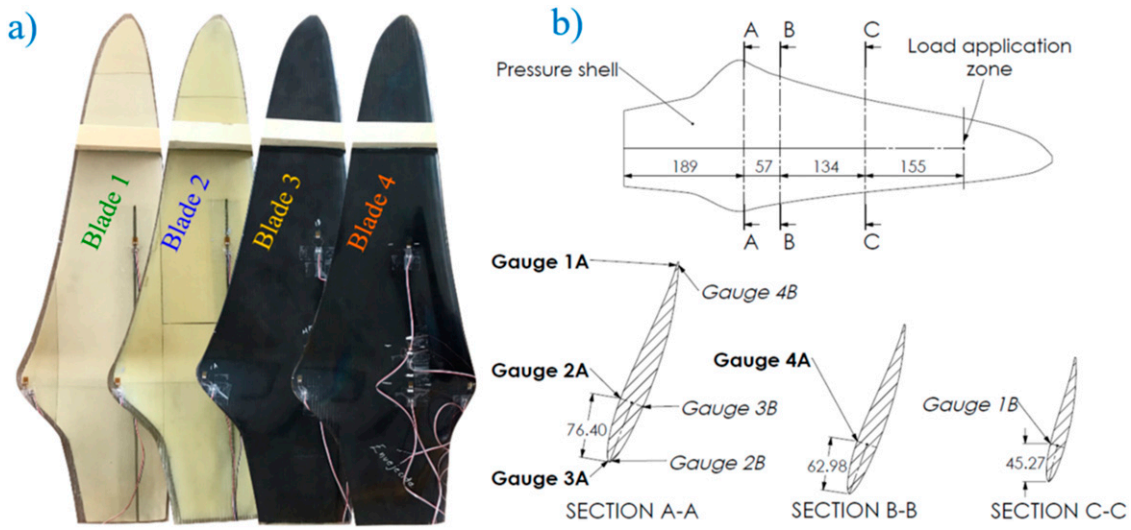

Figure 1. Scheme of a) manufactured blades and, b) diagraman of positions of the strain gauges. All dimensions are in mm.

Table 1. Blade description.

Manufactured by RTM process with PU core					
Label	Reinforcement	Matrix	MWCNTs (0.75% wt.)	Seawater aging	Length (mm)
Blade 1 (BD-1)	**Glass fiber**	**Epoxy resin**	No	No	670
Blade 2 (BD-2)			No	**Yes**	
Blade 3 (BD-3)			**Yes**	No	
Blade 4 (BD-4)			**Yes**	**Yes**	

Where W_t is the weight of the blade at a certain immersion time and W_0 is the initial weight of the blade before being submerged in seawater.

The artificial seawater was prepared by mixing 708.7 g of Morton Systems Saber II Pellets salt diluted in 20 L of purified water following the recommendations of previous studies.[23,60,62] This mixture reached a salinity of 36.8 psu (35.2%), similar to the seawater characteristics of the Gulf of Mexico.

Static structural testing

The static structural test of the blade was conducted on a test bench designed following the recommendations of the IEC-61400-23[63] y IEC TS 62600-3.[64] The test bench is equipped with a Futek FSH04080 load cell (USA) with a capacity of 22.5 kN, as well as a TE Connectivity displacement transducer with a measurement range of 0–1.27 m (see Figure 2). The load was applied using a steel cable wound around a pulley by the action of a Kollmorgen AKM54H-ACG2LB0W servo motor. During the test, values of applied force and displacement of the blade tip were recorded. Deformations were measured by 7 strain gauges attached to the surface of the blade. The gauges were distributed in a way that made it easy to monitor points of interest, as shown in Figure 1(b).

Electrical resistance measurement procedure

During static structural tests, the measurement of electrical resistance change was also carried out. The measurement of resistance change was only performed on the blades containing MWCNTs. For this purpose, the blades were instrumented with two pairs of electrodes consisting of thin copper wires attached to the surface of the blade and spaced 2 cm apart. The electrode's location coincided with the position of strain gauge 2B (see Figure 1(b)). To attach the wires to the surface of the blade, conductive silver paint from Ted Pella Inc (USA) was used, see Figure 3. The electrodes were attached to the suction side and the pressure side at the height of the maximum chord over the sparcap. The resistance change values were collected using a Keysight Truevolt 34465A digital multimeter connected to a computer via USB. For storage, a code generated using MatLab software was used. The sampling rate used was 1 Hz, and a multiplexer was employed to read both electrodes simultaneously. The relative change in electrical resistance (ΔR), was obtained using the equation (2), where

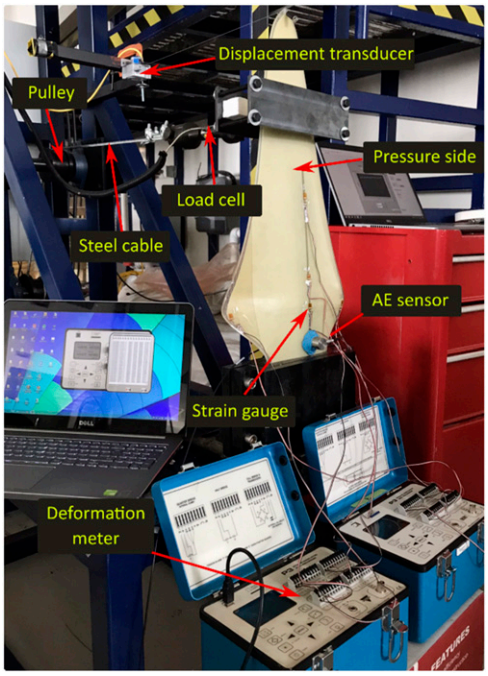

Figure 2. Instrumentation diagram for static testing of blades.

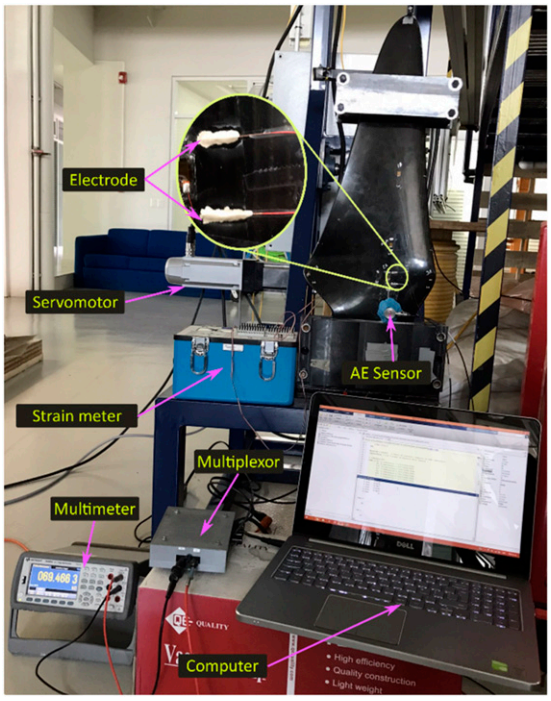

Figure 3. Instrumentation diagram of the blade for piezoresistive tests.

R_0 is the initial resistance and R_i is the value of the resistance measured during the static test.

$$\Delta R = \left(\frac{R_i - R_0}{R_0}\right) \times 100 \tag{2}$$

Acoustic emission technique

During the static structural test of the blade, damage was also monitored using the Acoustic Emission (AE) technique. For this purpose, a Micro-SHM System from Mistras Group Inc was used. Simultaneous measurements were conducted with two sensors at a frequency of 5 kHz. The sensors were placed at the root of the blade; one of them was attached to the pressure side, and the other to the suction side, as shown in Figure 3. During the damage monitoring test with AE, amplitude values over time were obtained. These data were collected from the beginning of the test until the maximum applied load.

Scanning electron microscopy

The coupons obtained from the tested blades, were examined by using a scanning electron microscope (SEM) JEOL JSM-6610LV operated at 15 kV at different magnifications. For this purpose, the coupons were coated with gold by sputtering. The aim was to analyze the damage mechanisms of the tested blade in the area with the greatest damage.

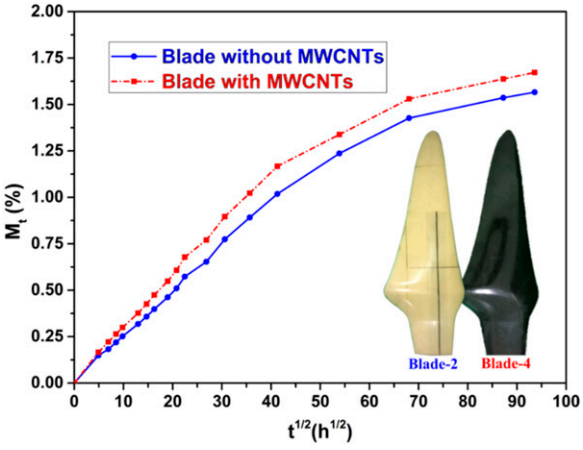

Figure 4. Moisture absorption results in blades with and without carbon nanotubes.

Results and discussion

Moisture absorption analysis

Figure 4 displays the results of the relative moisture absorption (M_t) as a function of the square root of time ($t^{1/2}(h^{1/2})$) of the blades that were submerged for 365 days in seawater. The graph shows a linear behavior at the beginning of the moisture absorption curve up to a time of

$30\,h^{1/2}$. This behavior is observed in both blades (without and with MWCNT) subjected to aging. The water absorption kinetics were fitted to the Fick's law behavior. After this time, the curves exhibited a non-linear behavior until the onset of a plateau at $t = 90\,h^{1/2}$, at this point, the blades begin to saturate with water. The moisture absorption is higher for the blade containing carbon nanotubes, which reached a maximum moisture absorption percentage of 1.67%, compared to 1.56% for the blades without carbon nanotubes. This behavior is directly related to the presence of carbon nanotubes in the fiber. This result of higher water absorption may be associated not only with the hydrophilic behavior of carbon nanotubes but also with the presence of small voids in the matrix due to the nanotubes, as well as the agglomeration and dispersion of the nanotubes, and the temperature of the seawater in which the elements were submerged.[60,65,66]

Performance of structural properties

The structural performance of the blades was evaluated through a static test, in which the blades with and without MWCNTs were tested under both dry and aged conditions. The design load obtained through numerical simulation was 789 N[59] and was applied in percentage intervals of 50, 70, 80, 90, and 110%,[63] resulting in a maximum applied load of 868 N, after reaching the maximum value of the load, a discharge of the applied load is carried out. All blades resisted 110% of the design load, although showing some variations in tip displacement and maximum deformation. These results are summarized in Table 1. It was observed that sample BD-4 showed a higher tip displacement with a value of 52 mm, this behavior is directly related to the higher percentage of moisture absorbed (see Figure 4) due to the presence of MWCNTs.[65] Moisture causes the matrix to plasticize and undergo hydrolysis,[67] making it ductile and less rigid,[68] in other words, the fiber-matrix interface undergoes imminent degradation (Figure 5). Similarly, blade BD-3 containing MWCNTs exhibits a higher tip displacement compared to blades without MWCNTs, suggesting that the presence of MWCNTs may lead to reduced blade stiffness.[69] In the case of blades without MWCNTs, the results show a smaller tip displacement (41.8 mm) for the unaged blade (BD-1) compared to the tip displacement (42.4 mm) for the aged blade (BD-2), see Figure 5. This is attributed to matrix plasticization caused by the seawater aging.[70] Seawater aging causes the displacement of the blade tip to increase by 1.43% in the case of blades without MWCNTs, while this increase is 13% in blades with MWCNT.

In relation to the strain measurements obtained with strain gauges attached to the surface of the blades, it can be observed that the non-aged blades (BD-1 and BD-3) exhibit higher strain readings compared to the aged blades (BD-2 and BD-4). This comparison is made at the position of strain gauge 4A (see Figure 1), the lower strain values in the aged blades are primarily attributed to inadequate load transfer from the point of load application to a distant strain measurement point, where strain gauge 4A is located, at a distance of 289 mm, this effect is related to matrix degradation.[71] However, when the strain measurement point (gauge 1B) is closer to the load application point (155 mm), the strain is higher in the aged blades. This reinforces the theory that load transfer to distant points from the load application point is not effective due to matrix degradation,[71] as seen in Figure 6. The presence of MWCNTs in the unaged blade (BD-3) causes greater deformation compared to the unaged blade without MWCNTs (BD-1). This can be observed by comparing the strains at gauges 4A and 1B in Figure 6, this difference is primarily attributed to the presence of MWCNTs in the matrix, and this behavior is consistent with the tip displacement of these blades. In the aged blades (BD-2 and BD-4), the presence of carbon nanotubes causes

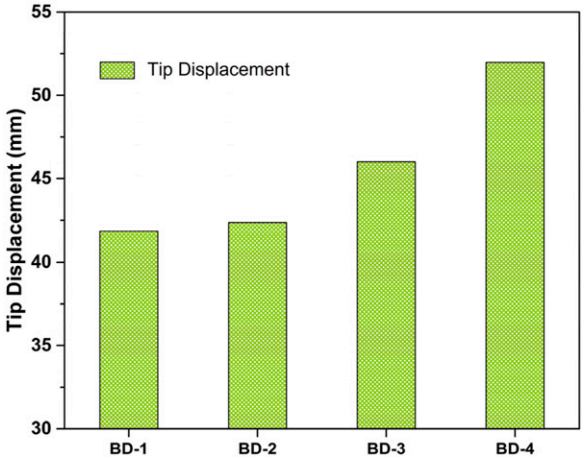

Figure 5. Tip displacement and strain values (4A gauge) of the tested blades.

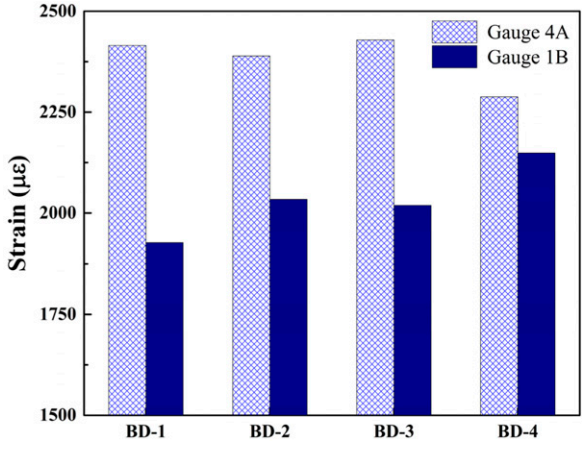

Figure 6. Strain values of gauge 4A and 1B of the tested blades.

Table 2. Summary of the results of static blade testing.

	MWCNTs (0.75% wt)	Condition	Max tip displacement (mm)	Max strain-gauge 4A (με)	Max strain-gauge 1B (με)
Blade (**BD-1**)	No	Dry	41.8	2415	1928
Blade (**BD-2**)	No	**Aged**	42.4	2389	2034
Blade (**BD-3**)	**Yes**	Dry	46.0	2429	2019
Blade (**BD-4**)	**Yes**	**Aged**	52.0	2288	2149

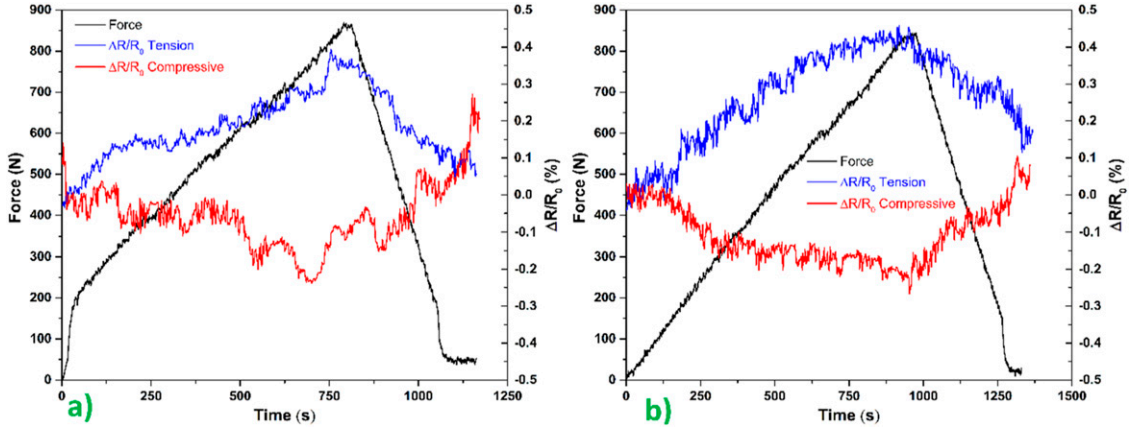

Figure 7. Piezoresistive curves of the blades with MWCNTs, (a) dry, (b) aged.

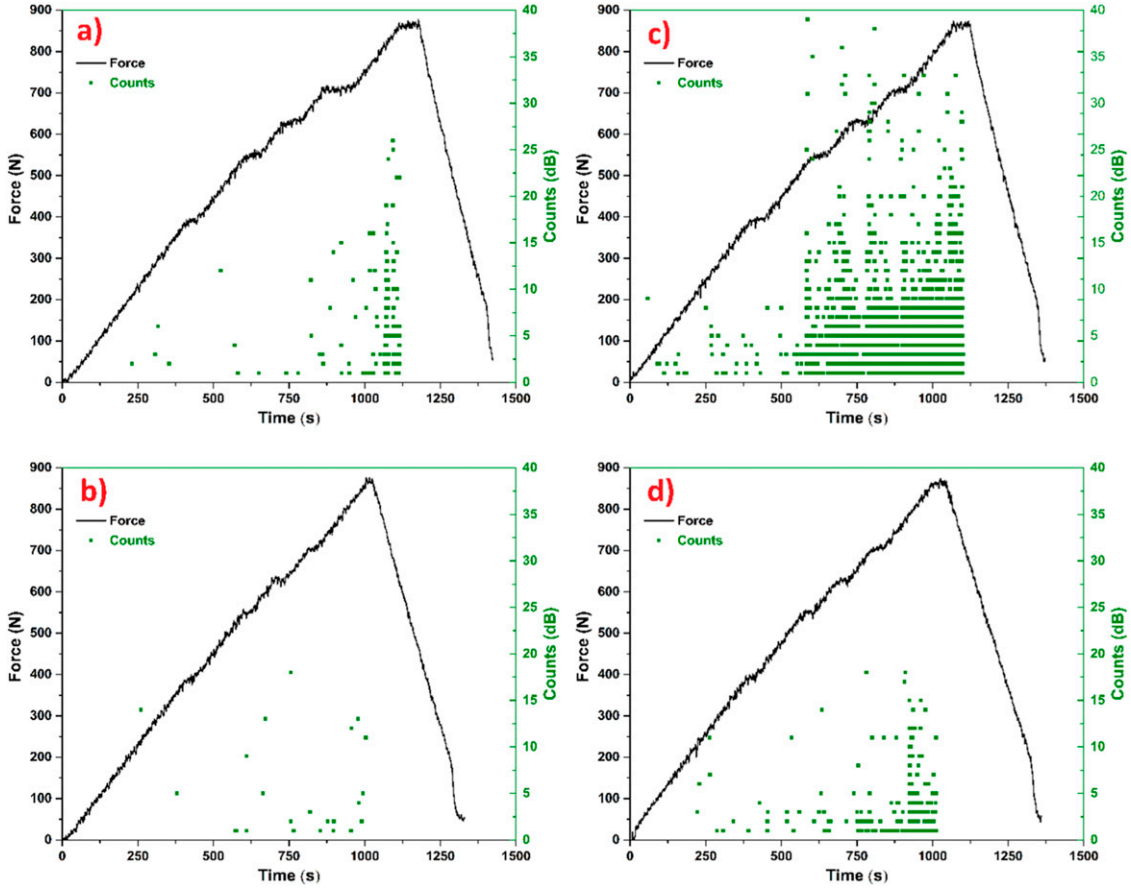

Figure 8. Results of AE in dry (left) and aged (right) blades, (a, c) blades without MWCNTs, (b, d) blades with MWCNTs.

greater deformation in the blade at the position of gauge 1B, which is closer to the load application point. This effect may be attributed to the presence of nanotubes and the degradation of the matrix due to absorbed seawater. Similarly, this behavior is consistent with the tip displacement of these blades. An inverse behavior can be observed in the strains at gauge 4A, which is farther from the load application point in the aged blades. This is attributed to the poor load transfer from the tip to distant load application points due to matrix degradation Table 2.

Electromechanical response

The electrical response of the blades was monitored during the static test. Electrical resistance measurements were taken from both aged and non-aged blades with MWCNTs. The electrical resistance relative change curves ($\Delta R/R_0$) are plotted against time (t) considering values from the electrodes placed on the compressive and tensile sides of the blade. The graphs also display the load values over time (see Figure 7). Figure 7(a) shows the results for the dry blade with MWCNTs, indicating a piezoresistive response to tension (blue line) and compression (red line), while there is a trend to follow the mechanical response in both electrical curves. Variations are also noticeable, which could be attributed to inherent noise in the properties of the nanotubes and the lack of robustness in the load application system. The maximum electrical resistance change value on the tensile side was 0.34%, and on the compressive side, a maximum of 0.23%. Regarding the piezoresistive response of the aged blades with MWCNTs, it is presented in Figure 7(b), the electrical curves also show a trend to follow the mechanical curve. Additionally, these curves exhibit some presence of noise. The maximum electrical resistance change value on the tensile side is 0.45%, and on the compressive side, 0.26%. According to these results, aged blades exhibit higher sensitivity in the electrical curves, which may be attributed to matrix plasticization, facilitating contact and the formation of the bridging effect[72,73] of the nanotubes when a load is applied, allowing for the formation or maintenance of the electrical network. It is also important to mention that a significant finding of this research was to demonstrate that the piezoresistive property of the blades can be preserved even after seawater aging. This may be a suitable technique for structural health monitoring of components exposed to marine environments.

Acoustic emission measurement

The Acoustic Emission (AE) monitoring was carried out during the static testing of the blades. The results are presented in Figure 8, where the amplitude values of counts (in dB) are plotted against time. Additionally, the curve of applied load versus time is included. The amplitude and quantity of counts are directly related to the level of noise produced by damage mechanisms during the static testing. In general, it is observed that the number of counts and amplitude increase as the applied force also increases. The greatest number of counts is observed when the maximum load is reached, and this behavior is observed in all the blades. According to the results, it can be observed that the aged blade without MWCNTs (Figure 8(c)) and the aged blade with MWCNTs (Figure 8(d)) exhibit a higher count density compared to the count density of the dry blades without and with carbon nanotubes (Figure 8(a) and (b)). This behavior suggests that the quantity of internal defects is higher in the aged blades, due to the weakening of the fiber–matrix interface caused by moisture. Another important finding was that in the dry blade without MWCNTs (Figure 8(a)) a higher density of counts was observed compared to the dry blade with MWCNTs (Figure 8(b)), this behavior could be explained by the presence of the MWCNTs, which, when interacting with the matrix, prevents the generation and propagation of micro-cracks caused by applied load. The same behavior was observed in the aged blades without MWCNTs when compared to the aged blades with MWCNTs, although the matrix is

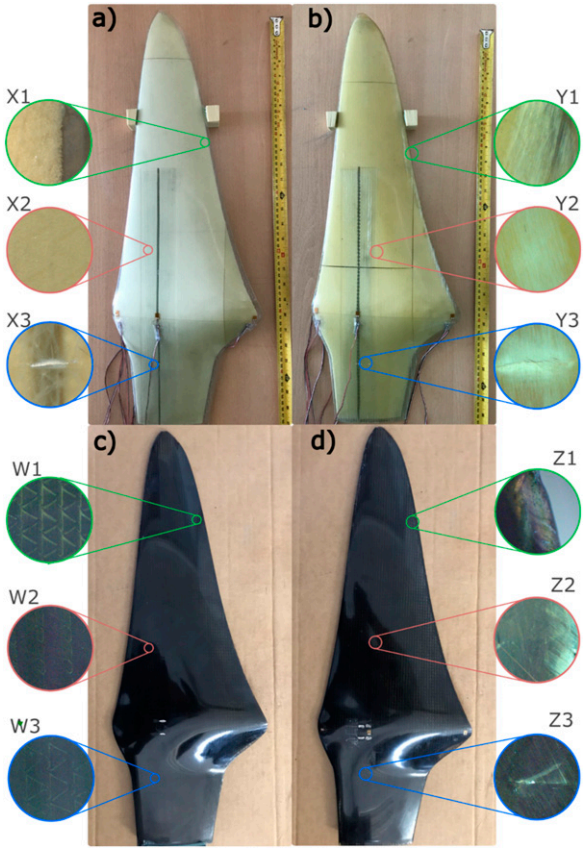

Figure 9. Visual inspection after structural test dry (left) and aged (right) blades, (a, b) without MWCNTs, (c, d) with MWCNTs.

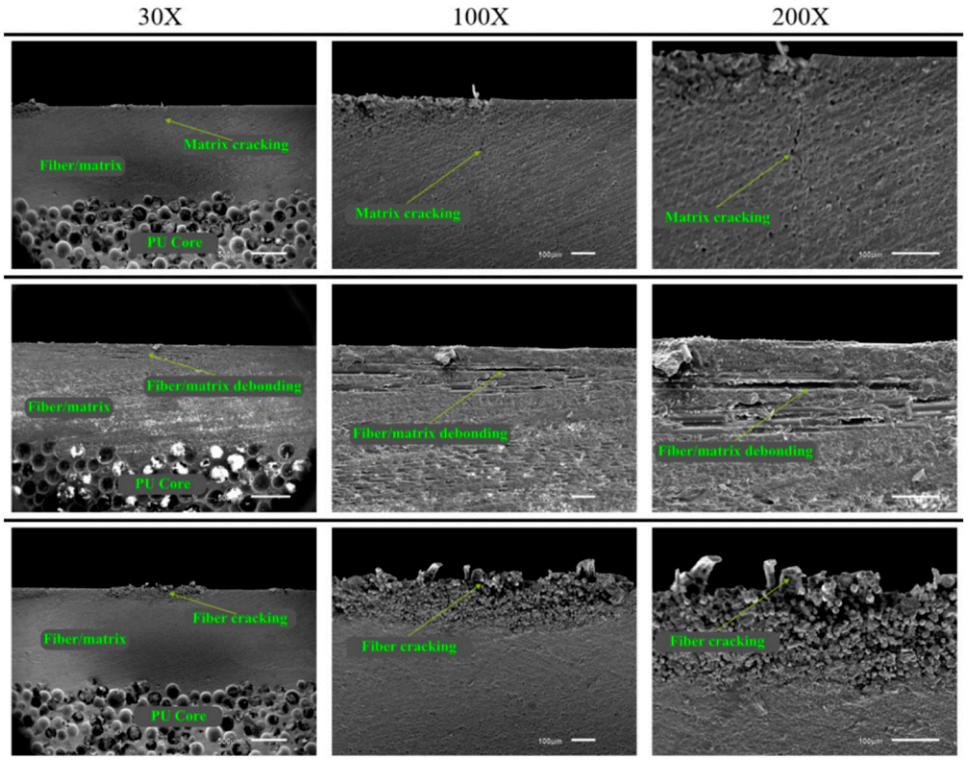

Figure 10. Fractography of damage zone on the aged blade without MWCNTs.

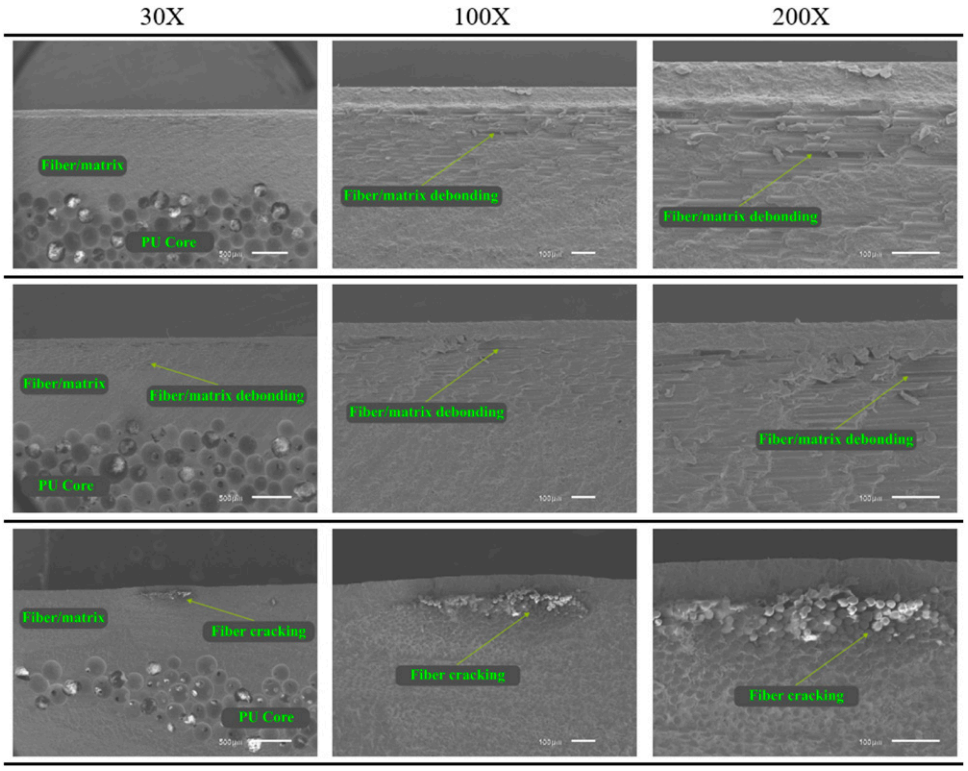

Figure 11. Fractography of damage zone on the aged blade with MWCNTs.

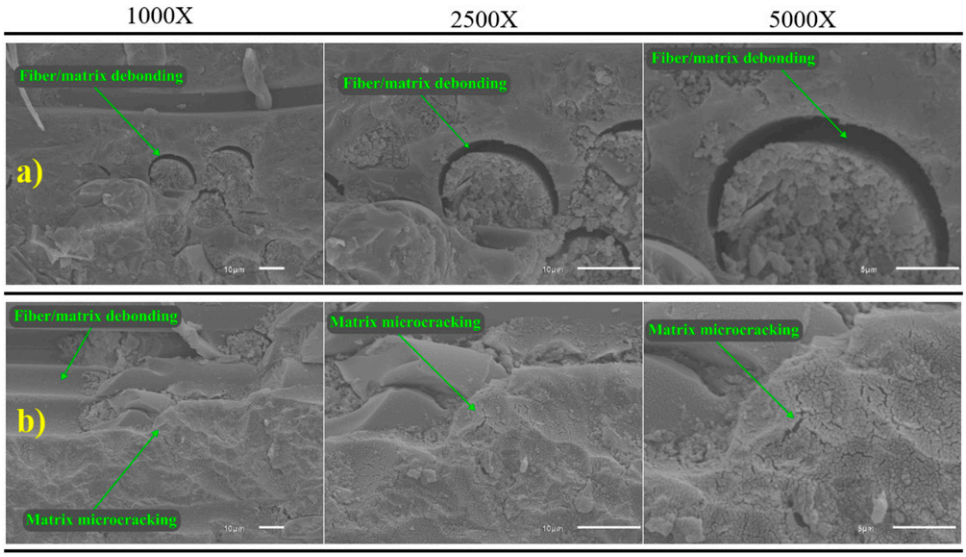

Figure 12. Fractography of damage mechanisms of aged blade, (a) fiber/matrix debonding, and (b) matrix microcracking.

degraded due to the effect of seawater, carbon nanotubes prevent damage mechanisms such as micro-cracks from propagating.

Analyzing the AE results in Figure 8, it is important to highlight that the greater acoustic activity exhibited by the wet sample without CNT (Figure 8(c)) is associated with all the damage mechanisms present in the composite material. Matrix cracking and debonding present lower energy and amplitude values compared to delamination and fiber breakage mechanisms,[49] and this fact is further verified by SEM observations of the failure surface. Aging in seawater causes the blades to present more acoustic and higher energy events during the bending test. Additionally, the acoustic events of wet blades occur early in time, while in dry blades they are slightly delayed.

Visual inspection and fractography of damage

After the structural static test, a visual inspection of the blades was conducted. Figure 9 provides a comparison of the damage in the blades without (Figure 9(a) and (b)) and with (Figure 9(c) and (d)) MWCNTs, and visual inspection of the blades without aging is also presented (Figure 9(a) and (c)) and with aging (Figure 9(b) and (d)). The first finding observed was the change in color of the matrix (yellowish) in the aged blade without MWCNTs (Figure 9(b)) due to the temperature of the seawater. While the blade with MWCNTs (Figure 9(d)), due to its appearance, it is difficult to appreciate the color change. Additionally, areas of internal color change in the blade without MWCNTs (Y1, Y2, see Figure 9(b)) were found, which may be due to the presence of damage mechanisms, these color changes can be observed to a lesser extent in the blade with MWCNTs, as can be seen in areas Z1 and Z2 of the Figure 9(d). These color changes are more evident in the edge area of the blades (Y1 and Z1) and over the sparcap area (Y2 and Z2), see Figure 9(b) and (d). Damages caused by the tooling, originating near the root of the blades, are also observed (Y3 and Z3). In the case of the unaged blades without MWCNTs (Figure 9(a)) significant damage could not be visually observed at first glance (X1, X2), only a small mark near the root area (X3) is noticeable, which is attributed to the contact between the blade and the testing tool. In the case of the blade with MWCNTs without aging, the damage caused by the static test cannot be seen with visual inspection, as shown in the Figure 9(d).

After visual inspection, coupons were extracted from the areas (Y1 and Z1) where the internal color change in the blades indicated the presence of greater internal damage, which needed to be verified by scanning electron microscopy inspection. The results demonstrate that there are different damage mechanisms such as matrix cracking, fiber/matrix debonding, and fiber breakage due to the load applied during the static test (see Figures 10 and 11). According to the results, the most frequently found damage mechanism is fiber/matrix debonding that causes the internal color change in the aged blade without MWCNTs (see Figure 10). Likewise, fiber breakage can be observed clearly near the external surface of the blade as well as matrix cracks. In the case of the blade aged with MWCNTs (see Figure 11), no matrix cracking damage was found, but damage mechanisms such as fiber/matrix debonding and fiber cracking can be seen, although to a lesser extent compared to the blade aged without MWCNTs.

On the other hand, Figure 12 shows images with different magnifications of the evidence found on the main damage mechanisms that occur due to seawater aging in the blades. In Figure 12(a), the presence of fiber/matrix debonding can

be seen in great detail, which occurs due to the swelling of the matrix caused by the difference in thermal expansion between the fiber and the matrix. Likewise, in Figure 12(b), the presence of micro-cracks in the matrix can be observed.

Conclusions

The effect of seawater aging on the mechanical performance of tidal turbine blades made of PU foam/fiberglass/epoxy composite was evaluated. The seawater-aged blade was subjected to flexural loading and damage monitoring was performed using acoustic emission and the self-sensing capability of the blade. The self-sensing capability was provided by the incorporation of MWCNT into the outer layer of the blade during the manufacturing process. Some relevant conclusions drawn from this research work are the following:

- Exposure of the blades with and without MWCNT to seawater caused a moisture absorption of 1.67% and 1.56%, respectively, inducing damage such as matrix cracking and debonding of the fiber/matrix interface. Furthermore, an increase in tip displacement of 13% and 1.43% was observed in the blades with and without MWCNT due to seawater aging.
- Despite the negative effects of seawater aging, the self-sensing capability of the blade was maintained, and the electrical resistance change approach enabled monitoring of strain and damage to the seawater-aged blade.
- Local damage due to seawater aging and applied load was observed on the blade, and the above-mentioned damage mechanisms were confirmed by SEM evaluation.
- Fewer acoustic emission (AE) events were observed in blades with MWCNT, suggesting that the presence of MWCNT acts as a hardening mechanism to reduce damage. On the other hand, blades aged in seawater exhibited more AE counts compared to the dry ones; confirming damage such as weakening of the fiber–matrix interface caused by humidity.

Therefore, it is worth mentioning, that the self-sensing capability induced by the incorporation of MWCNTs in combination with AE could be suitable non-destructive inspection techniques for SHM of marine components, such as tidal turbine blades.

Acknowledgments

The authors express their gratitude to Ing. Maria del Pilar Urquijo for her technical assistance in the acquisition of acoustic emission data, and to M. C. Miguel A. Vargas for his technical support in the weighing process of the blades.

Declaration of conflicting interests

The author(s) declared no potential conflicts of interest with respect to the research, authorship, and/or publication of this article.

Funding

The author(s) disclosed receipt of the following financial support for the research, authorship, and/or publication of this article: This work was financially supported by the "Centro Mexicano de Innovación en Energía del Océano" (CEMIE-O); 249795.

ORCID iDs

Eduardo José-Trujillo https://orcid.org/0000-0001-7027-9252
Julio A. Rodríguez-González https://orcid.org/0000-0001-7959-6203

Data availability statement

The data used to support the findings of this study are available from the corresponding author upon reasonable request.

Supplemental Material

Supplemental material for this article is available online.

References

1. Panwar NL, Kaushik SC and Kothari S. Role of renewable energy sources in environmental protection: a review. *Renew Sustain Energy Rev* 2011; 15: 1513–1524.
2. Apergis N and Payne JE. CO_2 emissions, energy usage, and output in Central America. *Energy Pol* 2009; 37: 3282–3286.
3. Winter RA. Innovation and the dynamics of global warming. *J Environ Econ Manag* 2014; 68: 124–140.
4. Menanteau P, Finon D and Lamy M-L. Prices versus quantities: choosing policies for promoting the development of renewable energy. *Energy Pol* 2003; 31: 799–812.
5. Fischer C and Newell RG. Environmental and technology policies for climate mitigation. *J Environ Econ Manag* 2008; 55: 142–162.
6. Paul A, Palmer K and Woerman M. Analysis of the Bingaman clean energy standard proposal. *Resour Energy Econ* 2014; 36: 113–129.
7. Bahaj AS. Generating electrical power from ocean resources. In: *Comprehensive renewable energy*. Amsterdam, the Netherlands: Elsevier, 2012, pp. 1–6.
8. Lange MA. Renewable energy and water resources. In: *Climate vulnerability*. Amsterdam, the Netherlands: Elsevier, 2013, pp. 149–166.
9. Mukhopadhyay R, Karisiddaiah SM and Mukhopadhyay J. Threat to opportunity. In: *Climate change*. Amsterdam, the Netherlands: Elsevier, 2018, pp. 99–117.
10. Marsh G. Tidal turbines harness the power of the sea. *Reinforc Plast* 2004; 48: 44–47.
11. Zhou HF, Dou HY, Qin LZ, et al. A review of full-scale structural testing of wind turbine blades. *Renew Sustain Energy Rev* 2014; 33: 177–187.
12. Finnegan W, Allen R, Glennon C, et al. Manufacture of high-performance tidal turbine blades using advanced composite manufacturing technologies. *Appl Compos Mater* 2021; 28: 2061–2086.
13. Tian W, Mao Z and Ding H. Design, test and numerical simulation of a low-speed horizontal axis hydrokinetic turbine. *Int J Nav Archit Ocean Eng* 2018; 10: 782–793.

14. Gonabadi H, Oila A, Yadav A, et al. Fatigue life prediction of composite tidal turbine blades. *Ocean Eng* 2022; 260: 111903.
15. Alam P, Robert C and Ó Brádaigh CM. Tidal turbine blade composites - a review on the effects of hygrothermal aging on the properties of CFRP. *Compos B Eng* 2018; 149: 248–259.
16. Murray R, Beach R, Murdy P, et al. *Structural characterization of deployed thermoplastic and thermoset composite tidal turbine blades*. Golden, CO: National Renewable Energy Laboratory, 2024.
17. Islam F, Caldwell R, Phillips AW, et al. A review of relevant impact behaviour for improved durability of marine composite propellers. *Composites Part C: Open Access* 2022; 8: 100251.
18. Li W, Zhou H, Liu H, et al. Review on the blade design technologies of tidal current turbine. *Renew Sustain Energy Rev* 2016; 63: 414–422.
19. Liu P and Veitch B. Design and optimization for strength and integrity of tidal turbine rotor blades. *Energy* 2012; 46: 393–404.
20. Walker SRJ, Thies PR and Johanning L. Comparative life cycle assessment of tidal stream turbine blades. *Int J Mar Ene* 2022; 5: 249–256.
21. Sathishkumar TP, Satheeshkumar S and Naveen J. Glass fiber-reinforced polymer composites – a review. *J Reinforc Plast Compos* 2014; 33: 1258–1275.
22. Rubino F, Nisticò A, Tucci F, et al. Marine application of fiber reinforced composites: a review. *JMSE* 2020; 8: 26.
23. José-Trujillo E, Rubio-González C and Rodríguez-González JA. Seawater ageing effect on the mechanical properties of composites with different fiber and matrix types. *J Compos Mater* 2019; 53: 3229–3241.
24. Zafar A, Bertocco F, Schjødt-Thomsen J, et al. Investigation of the long term effects of moisture on carbon fibre and epoxy matrix composites. *Compos Sci Technol* 2012; 72: 656–666.
25. Murray RE, Nevalainen T, Gracie-Orr K, et al. Passively adaptive tidal turbine blades: design tool development and initial verification. *International Journal of Marine Energy* 2016; 14: 101–124.
26. Shi W, Atlar M, Rosli R, et al. Cavitation observations and noise measurements of horizontal axis tidal turbines with biomimetic blade leading-edge designs. *Ocean Eng* 2016; 121: 143–155.
27. Gohil PP and Saini RP. Coalesced effect of cavitation and silt erosion in hydro turbines—a review. *Renew Sustain Energy Rev* 2014; 33: 280–289.
28. Hassan E. *Erosion issues in tidal turbine blades*. Glasgow, Scotland: University of Strathclyde, 2023.
29. Munaweera Thanthirige TR, Goggins J, Flanagan M, et al. A state-of-the-art review of structural testing of tidal turbine blades. *Energies* 2023; 16: 4061.
30. Jaksic V, Steynor J and O'Bradaigh C (eds) Tidal blade design and testing. In: 4th international conference on offshore renewable energy, CORE 2019, Glasgow, UK, September 2019.
31. Gonabadi H, Oila A, Yadav A, et al. Structural performance of composite tidal turbine blades. *Compos Struct* 2021; 278: 114679.
32. Fagan EM, Kennedy CR, Leen SB, et al. Damage mechanics based design methodology for tidal current turbine composite blades. *Renew Energy* 2016; 97: 358–372.
33. Kennedy CR, Leen SB and Ó Brádaigh CM. Immersed fatigue performance of glass fibre-reinforced composites for tidal turbine blade applications. *J Bio Tribo Corros* 2016; 2: 12.
34. Nachtane M, Tarfaoui M, Ait Mohammed M, et al. Effects of environmental exposure on the mechanical properties of composite tidal current turbine. *Renew Energy* 2020; 156: 1132–1145.
35. Davies P, Dumergue N, Arhant M, et al. Material and structural testing to improve composite tidal turbine blade reliability. *Int J Mar Ene* 2022; 5: 57–65.
36. Robin A, Arhant M, Davies P, et al. Effect of aging on the in-plane and out-of-plane mechanical properties of composites for design of marine structures. *Compos Part C: Open Access* 2023; 11: 100354.
37. Robin A, Davies P, Arhant M, et al. Mechanical performance of sandwich materials with reduced environmental impact for marine structures. *Jnl of Sandwich Struct & Mat* 2024; 26: 99–113.
38. Jiang Y, Finnegan W, Wallace F, et al. Structural analysis of a fibre-reinforced composite blade for a 1 MW tidal turbine rotor under degradation of seawater. *J Ocean Eng Mar Energy* 2023; 9: 1–18.
39. Aceti P, Carminati L, Bettini P, et al. Hygrothermal ageing of composite structures. Part 1: technical review. *Compos Struct* 2023; 319: 117076.
40. Xie T, Wang T, He Q, et al. A review of current issues of marine current turbine blade fault detection. *Ocean Eng* 2020; 218: 108194.
41. Mieloszyk M, Majewska K and Ostachowicz W. Application of embedded fibre Bragg grating sensors for structural health monitoring of complex composite structures for marine applications. *Mar Struct* 2021; 76: 102903.
42. Malekimoghadam R, Krause S and Czichon S. A critical review on the structural health monitoring methods of the composite wind turbine blades. In: Abdel Wahab M (ed) Proceedings of 1st international conference on structural damage modelling and assessment, Singapore, December 2021, pp. 409–438. Springer Singapore.
43. Chan T, Yu L, Tam HY, et al. Fiber Bragg grating sensors for structural health monitoring of Tsing Ma bridge: background and experimental observation. *Eng Struct* 2006; 28: 648–659.
44. Yeager M, Todd M, Gregory W, et al. Assessment of embedded fiber Bragg gratings for structural health monitoring of composites. *Struct Health Monit* 2017; 16: 262–275.
45. Zhou Z, Liu W, Huang Y, et al. Optical fiber Bragg grating sensor assembly for 3D strain monitoring and its case study in highway pavement. *Mech Syst Signal Process* 2012; 28: 36–49.
46. Zheng R, Liu L, Zhao X, et al. Investigation of measurability and reliability of adhesive-bonded built-in fiber Bragg grating sensors on steel wire for bridge cable force monitoring. *Measurement* 2018; 129: 349–357.
47. Tseranidis S, Theodoridis L, Loukogeorgaki E, et al. Investigation of the condition and the behavior of a modular floating structure by harnessing monitoring data. *Mar Struct* 2016; 50: 224–242.
48. Irfan MS, Khan T, Hussain T, et al. Carbon coated piezoresistive fiber sensors: from process monitoring to structural health monitoring of composites – a review. *Compos Appl Sci Manuf* 2021; 141: 106236.

49. Rubio-González C, de Urquijo-Ventura MP and Rodríguez-González JA. Damage progression monitoring using self-sensing capability and acoustic emission on glass fiber/epoxy composites and damage classification through principal component analysis. *Compos B Eng* 2023; 254: 110608.
50. He Y, Li M, Meng Z, et al. An overview of acoustic emission inspection and monitoring technology in the key components of renewable energy systems. *Mech Syst Signal Process* 2021; 148: 107146.
51. Zhang H, Bilotti E and Peijs T. The use of carbon nanotubes for damage sensing and structural health monitoring in laminated composites: a review. *Nanocomposites* 2015; 1: 167–184.
52. Rodríguez-González JA, Rubio-González C and Ku-Herrera JJ. Influence of seawater ageing on the mechanical and damage self-sensing capability of glass fiber-MWCNT/epoxy laminates subjected to flexural loading by means of the electrical resistance approach. *Smart Mater Struct* 2018; 27: 125002.
53. Rodríguez-González JA, Rubio-González C and Soto-Cajiga JA. Piezoresistive response of spray-coated multiwalled carbon nanotube/glass fiber/epoxy composites under flexural loading. *Fibers Polym* 2019; 20: 1673–1683.
54. Zhang H, Kuwata M, Bilotti E, et al. Integrated damage sensing in fibre-reinforced composites with extremely low carbon nanotube loadings. *J Nanomater* 2015; 2015: 1–7.
55. Lazaridou I, Kourkoulis SK and Alexopoulos ND. Damage monitoring of different concentration carbon nanotube/epoxy glass fiber reinforced composites under quasi-static incremental loadings. *Mater Today Proc* 2019; 12: 262–270.
56. Ma P-C, Siddiqui NA, Marom G, et al. Dispersion and functionalization of carbon nanotubes for polymer-based nanocomposites: a review. *Compos Appl Sci Manuf* 2010; 41: 1345–1367.
57. Li J, Ma PC, Chow WS, et al. Correlations between percolation threshold, dispersion state, and aspect ratio of carbon nanotubes. *Adv Funct Mater* 2007; 17: 3207–3215.
58. Li J and Kim J-K. Percolation threshold of conducting polymer composites containing 3D randomly distributed graphite nanoplatelets. *Compos Sci Technol* 2007; 67: 2114–2120.
59. Rubio-González C, José-Trujillo E, Alejandro Rodríguez-González J, et al. Strain self-sensing capability of a tidal turbine blade fabricated of PU-foam/glass fiber/epoxy composites using MWCNTs. *J Reinforc Plast Compos* 2023; 42: 363–376.
60. José-Trujillo E, Rubio-González C and Rodríguez-González JA. Evaluation of the piezoresistive response of GFRP with a combination of MWCNT and GNP exposed to seawater aging. *Appl Compos Mater* 2024; 31: 467–488.
61. ASTM D5229. *Test method for moisture absorption properties and equilibrium conditioning of polymer matrix composite materials*. West Conshohocken, PA: ASTM, 2020.
62. Rodríguez-González JA and Rubio-González C. Seawater effects on interlaminar fracture toughness of glass fiber/epoxy laminates modified with multiwall carbon nanotubes. *J Compos Mater* 2021; 55: 387–400.
63. IEC 61400-23. *Wind turbines generator systems – part 23: full-scale structural testing of rotor blades*. Geneva, Switzerland: IEC, 2014.
64. IEC TS 62600-3:2020. *Marine energy – wave, tidal and other water current converters – Part 3: measurement of mechanical loads*. Geneva, Switzerland: IEC, 2020.
65. Zulfli NM, Bakar AA and Chow WS. Mechanical and water absorption behaviors of carbon nanotube reinforced epoxy/glass fiber laminates. *J Reinforc Plast Compos* 2013; 32: 1715–1721.
66. Chamis CC. *Mechanics of load transfer at the fiber/matrix interface*. Cleveland, OH: NASA.
67. Colin X and Verdu J. Humid ageing of organic matrix composites. In: Davies P and Rajapakse YD (eds) *Durability of composites in a marine environment*. Dordrecht, the Netherlands: Springer Netherlands, 2014, pp. 47–114.
68. Yu B and Yang J. 1.20 hygrothermal effects in composites. In: *Comprehensive composite materials II*. Amsterdam, the Netherlands: Elsevier, 2018, pp. 502–519.
69. José-Trujillo E, Rubio-González C and Rodríguez-González JA. Study of seawater effect on the mechanical and thermomechanical properties of hybrid multiwall carbon nanotube/graphene nanoplatelet-glass fiber/epoxy laminates. *Polym Compos* 2022; 43: 8673–8686.
70. Hammami A and Al-Ghuilani N. Durability and environmental degradation of glass-vinylester composites. *Polym Compos* 2004; 25: 609–616.
71. Huang S, Fu Q, Yan L, et al. Characterization of interfacial properties between fibre and polymer matrix in composite materials – a critical review. *J Mater Res Technol* 2021; 13: 1441–1484.
72. Lu X, Yvonnet J, Detrez F, et al. Multiscale modeling of nonlinear electric conductivity in graphene-reinforced nanocomposites taking into account tunnelling effect. *J Comput Phys* 2017; 337: 116–131.
73. Gong S, Zhu ZH and Li Z. Electron tunnelling and hopping effects on the temperature coefficient of resistance of carbon nanotube/polymer nanocomposites. *Phys Chem Chem Phys* 2017; 19: 5113–5120.